[논 문] 한국재료학회지
Korean J. Mater. Res.
Vol. 29, No. 3 (2019)

https://doi.org/10.3740/MRSK.2019.29.3.150

Effect of MnO_2 and CuO Addition on Microstructure and Piezoelectric Properties of $0.96(K_{0.5}Na_{0.5})_{0.95}Li_{0.05}Nb_{0.93}Sb_{0.07}O_3$-$0.04BaZrO_3$ Ceramics

Kyung-Hoon Cho†

School of Materials Science and Engineering, Kumoh National Institute of Technology,
61 Daehak-ro, Gumi, Gyeongbuk 39177, Republic of Korea

(Received February 12, 2019 : Revised February 19, 2019 : Accepted February 20, 2019)

Abstract This study investigates the effect of MnO_2 and CuO as acceptor additives on the microstructure and piezoelectric properties of $0.96(K_{0.5}Na_{0.5})_{0.95}Li_{0.05}Nb_{0.93}Sb_{0.07}O_3$-$0.04BaZrO_3$, which has a rhombohedral-tetragonal phase boundary composition. MnO_2 and CuO-added $0.96(K_{0.5}Na_{0.5})_{0.95}Li_{0.05}Nb_{0.93}Sb_{0.07}O_3$-$0.04BaZrO_3$ ceramics sintered at a relatively low temperature of 1020 °C show a pure perovskite phase with no secondary phase. As the addition of MnO_2 and CuO increases, the sintered density and grain size of the resulting ceramics increases. Due to the difference in the amount of oxygen vacancies produced by B-site substitution, Cu ion doping is more effective for uniform grain growth than Mn ion doping. The formation of oxygen vacancies due to B-site substitution of Cu or Mn ions results in a hardening effect via ferroelectric domain pinning, leading to a reduction in the piezoelectric charge coefficient and improvement of the mechanical quality factor. For the same amount of additive, the addition of CuO is more advantageous for obtaining a high mechanical quality factor than the addition of MnO_2.

Key words Pb-free, piezoelectric, acceptor doping, hardening, oxygen vacancy.

1. Introduction

Piezoelectric materials that enable mutual conversion between electrical energy and mechanical energy are widely used as transducer elements such as actuators, ignitors, filters, sound generators, and sensors. Most modern piezoelectric devices are composed of lead-rich materials such as $PbZr_{1-x}Ti_xO_3$-based and $Pb(Mg_{1/3}Nb_{2/3})O_3$-based compositions. As regulations such as the Restriction of Hazardous Substances(RoHS) of the European Union are gradually expanded, the development of lead-free piezoelectric ceramics is actively underway.[1-10)]

Among the various candidates for use as lead-free piezoelectric ceramics, $(K,Na)NbO_3$ (KNN)-based compositions have been most actively studied due to their good piezoelectric properties and high Curie temperatures.[11-14)] Many prior investigations have revealed that the orthorhombic-tetragonal phase transition temperature of KNN-based ceramics can be lowered to room temperature by substituting various elements into the A- and B-sites of the perovskite structure(ABO_3) and forming (1-x)KNN-xABO_3 solid solutions(A = Li, Ba, Sr, etc.; B = Ta, Sb, Ti, etc.), resulting in the enhancement of their piezoelectric properties.[11,15-18)] However, since these compositions exist in a polymorphic phase transition state, their piezoelectric performance will decrease if the temperature varies even slightly from room temperature. Recently, research into improving piezoelectric performance and temperature stability by designing rhombohedral-tetragonal phase boundary compositions has been reported.[19-22)] These compositions are designed to increase the rhombohedral-orthorhombic transition temperature and lower the orthorhombic-tetragonal transition temperature by doping appropriate elements into the KNN A-site and B-site, so that these two transition temperatures coincide at near-room temperature.

The compositional modifications described above are very attractive and technologically important for the development of high-performance lead-free piezoelectric materials. Further, studying the effect of additives on the lead-free materials being developed would be meaningful in terms of application to various piezoelectric devices.

†Corresponding author
E-Mail : khcho@kumoh.ac.kr (K.-H. Cho, Kumoh Nat'l Inst. Tech.)

In this study, we investigated the effect of MnO_2 and CuO as acceptor additives on the microstructure and piezoelectric properties of $0.96(K_{0.5}Na_{0.5})_{0.95}Li_{0.05}Nb_{0.93}Sb_{0.07}O_3$-$0.04BaZrO_3$ (KNLNS-BZ), which has a rhombohedral-tetragonal phase boundary composition. The microstructural changes induced by the acceptor additives and the resultant piezoelectric properties of specimens sintered at the relatively low temperature of 1,020 °C are discussed in terms of defect formation.

2. Experimental Procedure

To prepare the KNLNS-BZ piezoelectric material, reagent-grade raw K_2CO_3, Na_2CO_3, Li_2CO_3, Nb_2O_5, Sb_2O_3, and $BaCO_3$ powders(Kojundo Korea Co.) were mixed according to the stoichiometric composition and milled with ethanol and yttria-stabilized zirconia(YSZ) balls in a polyethylene jar for 24 h. Subsequently, the powder mixture was calcined at 850 °C for 6 h. Then, x mol% of MnO_2 or CuO (x = 0, 0.5, 1.0, or 1.5) was added to the calcined powder before a second ball-milling process. The second ball-milling was carried out using ethanol and YSZ balls for 72 h, after which the powder mixture was dried at 80 °C. The dried powder was pressed into a disk-shaped green body under 100 MPa, and the green body was sintered at 1,020 °C for 3 h in an air atmosphere. The bulk density of the sintered specimens was measured using the Archimedes method. An Ag electrode was formed on the top and bottom surfaces of the sintered specimens, and an electrical poling process was conducted by applying a DC electric field of 3 kV/mm for 30 min at room temperature in a silicone oil bath. The structural properties of the sintered specimens were characterized using X-ray diffraction(XRD, D-MAX/2500, Rigaku) and scanning electron microscopy(SEM, JSM-6500F, JEOL), and the piezoelectric properties were measured using a d_{33}-meter (YE2730A, Sinocera Piezotronics) and an impedance analyzer(IM3570, Hioki).

3. Result and Discussion

Fig. 1 shows the powder XRD patterns of the KNLNS-BZ, KNLNS-BZ + 1.5 mol% MnO_2, and KNLNS-BZ + 1.5 mol% CuO ceramics sintered at 1,020 °C. A perovskite structure without a secondary phase was observed for all the compositions, confirming that the Mn and Cu ions were well-substituted into the crystal lattice. The shapes of the (200) peak of the three specimens look slightly different from each other, meaning that there might be an effect of the additives on the phase change of the specimens. For pure KNLNS-BZ ceramic, the fraction of the tetragonal phase appears to be higher than that of the rhombohedral phase. For the other specimens containing additives, the fraction of the rhombohedral phase looks slightly increased.

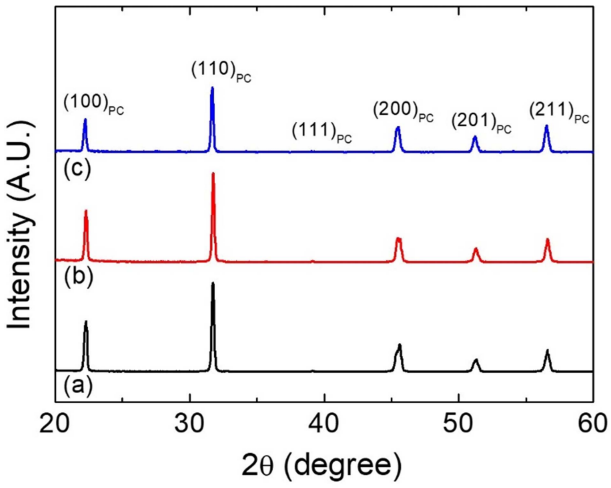

Fig. 1. X-ray diffraction patterns of the (a) $0.96(K_{0.5}Na_{0.5})_{0.95}Li_{0.05}Nb_{0.93}Sb_{0.07}O_3$-$0.04BaZrO_3$ ceramic, (b) $0.96(K_{0.5}Na_{0.5})_{0.95}Li_{0.05}Nb_{0.93}Sb_{0.07}O_3$-$0.04BaZrO_3$ + 1.5 mol% MnO_2 ceramic, and (c) $0.96(K_{0.5}Na_{0.5})_{0.95}Li_{0.05}Nb_{0.93}Sb_{0.07}O_3$-$0.04BaZrO_3$ + 1.5 mol% CuO ceramic.

Fig. 2 shows the surface SEM images of the KNLNS-BZ, KNLNS-BZ + 1.5 mol% MnO_2, and KNLNS-BZ + 1.5 mol% CuO ceramics sintered at 1,020 °C. As can be seen in Fig. 2(a), the pure KNLNS-BZ ceramic showed a very small grain size(200-300 nm) and little densification of the specimen occurred. However, when 1.5 mol% MnO_2 was added, grain growth was observed, as shown in Fig. 2(b), and a microstructure in which abnormal grains larger than 5 μm and normal grains of 0.5 to 3 μm coexisted was observed. When 1.5 mol% of CuO was added, a dense microstructure with overall grain growth was observed, and a relatively uniform grain size of 3 to 5 μm was obtained[Fig. 2(c)]. Therefore, both MnO_2 and CuO were found to be effective in lowering the sintering temperature of KNLNS-BZ ceramics. The CuO-containing specimen showed a larger overall grain size than the MnO_2-containing specimen despite the same amount of each being added; this can be interpreted as follows. Mn^{4+} and Cu^{2+} ions have ionic radii (r_i) of 0.67 Å and 0.87 Å, respectively, when the coordination number is 6. When these ions are doped into the KNLNS-BZ ceramics, they can enter the Nb^{5+} (r_i = 0.78 Å) or Zr^{4+} (r_i = 0.86 Å) ion sites (B-site), which have similar ionic radii. The expected incorporation reactions are as follows:

$$2MnO_2 \rightarrow 2Mn'_{Nb} + 4O_O + V_O^{oo} \quad (1)$$

$$2CuO \rightarrow 2Cu'''_{Nb} + 2O_O + 3V_O^{oo} \quad (2)$$

$$MnO_2 \rightarrow Mn_{Zr} + 2O_O \quad (3)$$

$$CuO \rightarrow Cu''_{Zr} + O_O + V_O^{oo} \quad (4)$$

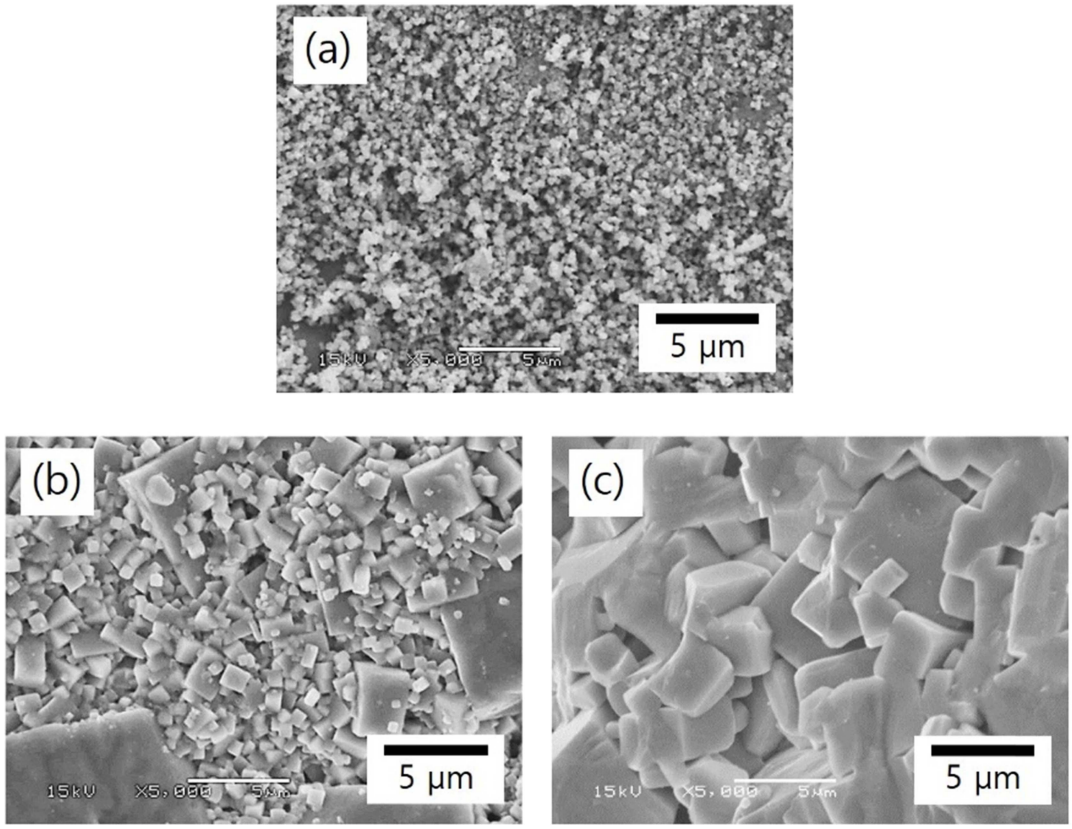

Fig. 2. SEM images of (a) $0.96(K_{0.5}Na_{0.5})_{0.95}Li_{0.05}Nb_{0.93}Sb_{0.07}O_3$-$0.04BaZrO_3$ ceramic, (b) $0.96(K_{0.5}Na_{0.5})_{0.95}Li_{0.05}Nb_{0.93}Sb_{0.07}O_3$-$0.04BaZrO_3$ + 1.5 mol% MnO_2 ceramic, and (c) $0.96(K_{0.5}Na_{0.5})_{0.95}Li_{0.05}Nb_{0.93}Sb_{0.07}O_3$-$0.04BaZrO_3$ + 1.5 mol% CuO ceramic.

As can be seen from the above equations, the addition of CuO contributes more to increasing the oxygen vacancy concentration than the addition of MnO_2. Since divalent and trivalent Mn ions coexist in manganese oxide above 870 °C, if the reaction starts at a high temperature, both Mn^{3+} and Mn^{2+} can enter the B-site together.[23,24] However, the total oxygen vacancy concentration in this case is still inevitably lower than when CuO is added. The sites with large ionic radii in the perovskite (ABO_3) structure are the A-site and O-site. Thus, as the concentration of oxygen vacancies increases, the thermal energy required for atomic diffusion may decrease, thereby increasing sinterability. Here, Schottky pair formation by A-site alkali-metal ions is not considered because the formation of oxygen vacancies compensates for the charged defects created by acceptor doping. In addition, since the specimens were sintered at a relatively low temperature of 1,020 °C, it is assumed that the volatilization of alkali-metal ions was not severe.

Fig. 3 shows the bulk density and piezoelectric properties of the specimens sintered at 1,020 °C according to the amount of MnO_2 or CuO added. For both MnO_2 and CuO, the density increased rapidly up to 94.7 % and 96.9 % of the theoretical density, respectively, as the additive

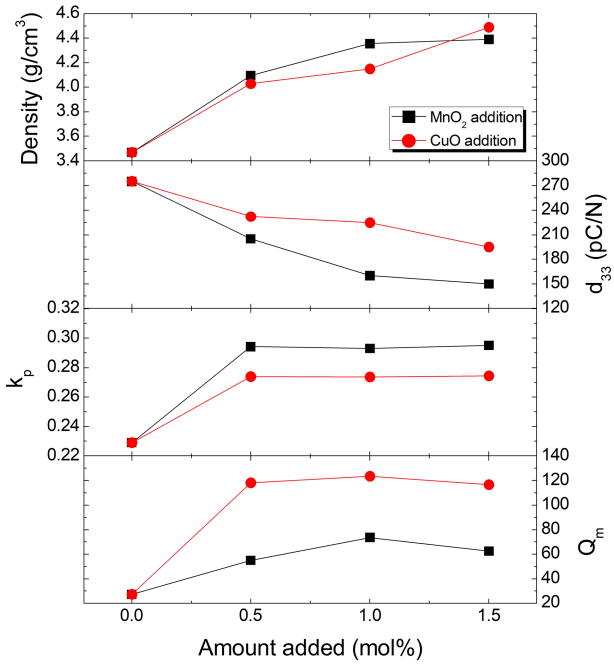

Fig. 3. Density, piezoelectric charge coefficient (d_{33}), electromechanical coupling coefficient (k_p), and mechanical quality factor (Q_m) of the $0.96(K_{0.5}Na_{0.5})_{0.95}Li_{0.05}Nb_{0.93}Sb_{0.07}O_3$-$0.04BaZrO_3$ ceramics sintered at 1,020 °C as a function of the amount of MnO_2 or CuO added.

amount increased. This was possibly due to the increase in the sinterability due to the increased oxygen vacancy concentration. However, the piezoelectric charge coefficient (d_{33}) showed a trend opposite to that of density. The pure KNLNS-BZ ceramic showed a high d_{33} value of 275 pC/N despite its very low bulk density, but d_{33} decreased gradually as the amount of additive increased. The d_{33} values of the ceramics with 1.5 mol% MnO_2 and 1.5 mol% CuO were 150 pC/N and 195 pC/N, respectively. The MnO_2-containing composition shows a more rapid decrease in d_{33} than the CuO-containing composition, seemingly because of the difference in the average grain size of the high-density specimens. As shown in Fig. 2, overall grain growth occurred well in the CuO-containing composition, and this might be the reason why d_{33} of the CuO-containing composition is maintained higher than that of MnO_2-containing composition, which had a relatively small average grain size.

The electromechanical coupling coefficient (k_p) increased sharply upon the addition of 0.5 mol% of additive compared to that of the pure KNLNS-BZ ceramic; however, no remarkable change in k_p was observed with an increase in the amount of additive. Low k_p values of less than 0.3 were obtained for all specimens. This result and the decrease in the d_{33} values demonstrate the hardening effect of the piezoelectrics. As described in Eqs. (1), (2), and (4), oxygen vacancies are formed for charge compensation when the substituted ions are lower-valent ions. Resulting oxygen vacancies pair with dopant ions and form chains parallel to one of the crystallographic axes. These chain fragments interact with the lower valent species, making it difficult to change the polarization due to the domain pinning effect. As a result, the d_{33} and k_p values of the acceptor ion-substituted compositions are smaller than those of the pure KNLNS-BZ ceramic. The small k_p value of the pure KNLNS-BZ ceramic in Fig. 3 was attributed to its very porous microstructure with a very small grain size. The hardening effect due to the presence of oxygen vacancies led to an increase in the mechanical quality factor (Q_m). As can be seen in Fig. 3, the Q_m value of the compositions increased sharply as the amount of MnO_2 or CuO added increased. The CuO-containing compositions showed much higher Q_m values than those of the MnO_2-containing compositions, again confirming that the oxygen vacancy concentration of the CuO-containing compositions was higher than that of the MnO_2-containing compositions.

4. Conclusion

In this study, the effect of the addition of MnO_2 and CuO on the sinterability and piezoelectric properties of KNLNS-BZ ceramics was investigated. Both MnO_2 and CuO promoted the grain growth of KNLNS-BZ ceramics, but the addition of CuO was more effective in inducing uniform grain growth. As the amount of MnO_2 or CuO added increased, the density and Q_m values increased rapidly, but d_{33} decreased and k_p remained low. This was interpreted as a hardening phenomenon due to the presence of oxygen vacancies. For the same amount of additive, it was found that the addition of CuO was more advantageous for obtaining a high d_{33} and Q_m at the same time than the addition of MnO_2.

Acknowledgement

This research was supported by Kumoh National Institute of Technology (2017-104-014).

References

1. T. Takenaka and H. Nagata, J. Eur. Ceram. Soc., **25**, 2693 (2005).
2. M. Kosec, B. Malic, A. Bencan and T. Rojac, KNN-based piezoceramics: In Piezoelectric and Acoustic Materials of Transducer Applications, A. Safari and E. K. Akdogan Eds., Springer Science and Business Media LLC, New York (2008).
3. J. Rödel, A. B. N. Kounga, M. Weissenberger-Eibl, D. Koch, A. Bierwisch, W. Rossner, M. J. Hoffmann, R. Danzer and G. Schneider, J. Eur. Ceram. Soc., **29**, 1549 (2009).
4. J. Rödel, W. Jo, K. Seifert, E. M. Anton, T. Granzow and D. Damjanovic, J. Am. Ceram. Soc., **89**, 1153 (2009).
5. T. R. Shrout and S. Zhang, J. Electroceram., **19**, 111 (2007).
6. D. Damjanovic, N. Klein, J. Li and V. Porokhonskyy, Funct. Mater. Lett., **3**, 5 (2010).
7. H. Y. Park, K. H. Cho, D. S. Paik, S. Nahm, H. G. Lee and D. H. Kim, J. Appl. Phys., **102**, 124101 (2007).
8. H. C. Song, K. H. Cho, H. Y. Park, C. W. Ahn, S. Nahm, K. Uchino and S. H. Park, J. Am. Ceram. Soc., **90**, 1812 (2007).
9. X. J. Cheng, J. G. Wu, X. P. Wang, D. Q. Xiao and J. G. Zhu, Appl. Phys. Lett., **103**, 052906 (2013).
10. T. Zheng, J. Wu, D. Xiao, J. Zhu, X. Wang and X. Lou, J. Mater. Chem. A, **3**, 1868 (2015).
11. Y. Saito, H. Takao, T. Tani, T. Nonoyama, K. Takatori, T. Homma, T. Nagaya and M. Nakamura, Nature, **432**, 84 (2004).
12. S. Zhang, R. Xia and T. R. Shrout, J. Electroceram., **19**, 251 (2007).
13. X. Wang, J. Wu, D. Xiao, J. Zhu, X. Cheng, T. Zheng, B. Zhang, X. Lou and X. Wang, J. Am. Chem. Soc., **136**, 2905 (2014).
14. M. H. Zhang, H. C. Thong, Y. X. Lu, W. Sun, J.-F. Li and K. Wang, J. Korean Ceram. Soc., **54**, 261 (2017).
15. K. Wang, J. F. Li and N. Liu, Appl. Phys. Lett., **93**,

092904 (2008).
16. J. Wu, Y. Wang, D. Xiao, J. Zhu, P. Yu, L. Wu and W. Wu, Jpn. J. Appl. Phys., **46**, 7375 (2007).
17. Y. F. Chang, Z. Yang, D. Ma, Z. Liu and Z. Wang, J. Appl. Phys., **104**, 024109 (2008).
18. J. H. Yoo and G. M. Lee, Trans. Electr. Electron. Mater., **19**, 375 (2018).
19. X. Cheng, J. Wu, X. Lou, X. Wang, X. Wang, D. Xiao and J. Zhu, ACS Appl. Mater. Interfaces, **6**, 750 (2014).
20. T. Zheng, J. Wu, X. Cheng, X. Wang, B. Zhang, D. Xiao and J. Zhu, Dalton Trans., **43**, 9419 (2014).
21. B. Zhang, J. Wu, X. Cheng, X. Wang, D. Xiao, J. Zhu, X. Wang and X. Lou, ACS Appl. Mater. Interfaces, **5**, 7718 (2013).
22. J. Wu, J. Xiao, T. Zheng, X. Wang, X. Cheng, B. Zhang, D. Xiao and J. Zhu, Scr. Mater., **88**, 41 (2014).
23. F. Shenouda and S. Aziz, J. Appl. Chem., **17**, 258 (1967).
24. K. H. Cho, C. S. Park and S. Priya, Appl. Phys. Lett., **97**, 182902 (2010).